J Mater Sci (2011) 46:1870–1876
DOI 10.1007/s10853-010-5015-1

Carbon nanofibers prepared by a novel co-extrusion and melt-spinning of phenol formaldehyde-based core/sheath polymer blends

Kuo-Kuang Cheng · Tzu-Chien Hsu · Li-Heng Kao

Received: 25 September 2010 / Accepted: 18 October 2010 / Published online: 30 October 2010

Abstract A novel route based on the solvent-free core/sheath melt-spinning of polypropylene/(phenol formaldehyde–polyethylene) [PP/(PF–PE)] to prepare the carbon nanofiber (CNF) has been demonstrated in this study. The approach consists of three main steps: co-extrusion of PP (core) and a polymer blend of PF and PE (sheath), followed by melt-spinning, to form the core/sheath fiber, stabilization of core/sheath fiber to form the carbon fiber precursor, and carbonization of carbon fiber precursor to form the final CNF. Both scanning electron microscopy and transmission electron microscopy images reveal long and winding CNF with diameter 100–600 nm and length greater than 80 μm. With a yield of ~45% based on its raw material PF, the CNF exhibits regularly oriented bundles which curl up to become rolls of wavy long fibers with clean and smooth surface. Results from X-ray diffractometry, Raman spectroscopy, and selected area electron diffraction pattern further reveal that the CNF exhibits a mixed-phase carbon material with graphitic particles embedded homogeneously in an amorphous carbon matrix.

K.-K. Cheng · T.-C. Hsu (✉)
Department of Materials and Optoelectronic Science,
National Sun Yat-Sen University, Kaohsiung 80424, Taiwan
e-mail: tjhsu@facmail.nsysu.edu.tw
URL: http://www.mse.nsysu.edu.tw/people/bio.php?

L.-H. Kao
Department of Chemical and Materials Engineering,
National Kaohsiung University of Applied Science,
Kaohsiung 80778, Taiwan

Introduction

The ultra-fine carbon fibers can be divided into two groups according to their structure and size: the carbon nanotube (CNT) and carbon nanofiber (CNF) [1–6]. Generally speaking, CNTs are hollow ultra-fine carbon fibers with diameters smaller than 20 nm; while CNFs are solid ultra-fine carbon fibers with diameters 20–1000 nm. Due to their high tenacity, light weight, and high heat and electric conductivity, and most importantly with high crystallinity, these ultra-fine carbon fibers have long been widely applied as functional materials or reinforcement materials in all kinds of composites. For instance, poly(epsilon-caprolactone)/CNF composite mats and films were prepared by electro-spinning and solvent casting [7–9]. On the other hand, the amorphous CNFs have attracted much attention in recently for their potential applications in the optoelectronic areas such as the hydrogen storage materials and as the electrode materials in lithium ion batteries.

There are two processes for producing ultra-fine carbon fibers, namely, the vapor-grown approach and the polymer solution spinning approach. The vapor-grown approach is a relatively simple but expensive one which may involve laser vaporization, arc discharge, or chemical vapor deposition [10–12]. The vapor-grown CNFs have been reported as ultra-fine carbon filaments which possess high crystallinity with high modulus and strength suitable for mechanical applications. The polymer solution spinning approach is adopted from a wet electro-spinning process well-known for producing polymeric fibers having submicron level; unfortunately, large amount of solvent is required, causing serious environmental problem. The wet polymer spinning approach to both CNT and CNF has been intensively investigated in recent years [13, 14]. In a study using single polymer precursor, a carbon precursor

polymer solution was first prepared; it was then processed by the typical electro-spinning process to give the polymer nanofibers. Carbonization of polymer nanofibers at a given temperature range of 400–1500 °C under nitrogen atmosphere resulted in the desired ultrafine carbon fibers with diameter of 90–600 nm. The carbon precursor polymers study included polyimide and polyacrylonitrile [15, 16]. On the other hand, a series of study by Oya et al. utilizing the core/shell microspheres which were made of various polymer blends with solvent to produce CNF with 200–300 nm in diameter were reported [17–20]. In their approach, a carbon precursor polymers/acetone solution was first sprayed and dispersed into a mixture solution containing a thermally decomposable polymer and toluene to form the core/shell microspheres having a carbon precursor polymers core. In this case, high-density polyethylene and novolac-type phenol–formaldehyde resin were used as the thermally decomposable polymer and the carbon precursor polymer, respectively. These core/shell particles were subsequently elongated by melt-spinning with the aid of a thermally decomposable polymer chip, stabilized in solution containing hydrochloric acid and formaldehyde, and finally converted to CNF after removing the thermally decomposable polymer during the subsequent carbonization process. Similar approach with the same raw materials and solvents were also applied for the preparation of CNT in which fine thermally decomposable polymer core particles with a carbon precursor polymer shell were spun and elongated; further removal of the thermally decomposable polymer core during carbonization yielded the CNT [21, 22]. In all the study mentioned above, it is noted that solvents such as acetone and toluene were required in both core and shell parts during the precursor preparation process.

This study adopts a new approach for making CNF by core/sheath melt-spinning without solvent, which is significantly different from the wet electro-spinning and wet polymer spinning reported [14–22]. There are three steps involved: (1) co-extrusion of the polypropylene (PP) as the core material and a blend of PF and PE as the sheath material, followed by melt-spinning, to form the PP/(PF–PE) core/sheath fiber (CSF); (2) stabilization of CSF to form a carbon fiber precursor (CFP); and (3) carbonization of CFP to obtain the CNF. From the material design point of view, it should be emphasized that PP as the core material plays a crucial role in providing the stability of CSF, whereas incorporation of PE into the carbon precursor PF to form the PF–PE blend is to ensure the spin ability of CSF during the melt-spinning process. This solvent-free approach involves no microspheres, and it yields CNF with different morphology and microstructure of carbon materials from those by the wet electro-spinning approach.

Experimental

Materials

PF (Novolac type, Dynea Singapore PTE Ltd), PE (Lotrene MG70, Qapco Ltd), and PP (Pro-fax PT231, Taiwan Polypropylene Co, Ltd) were used as received. Hydrochloric acid (HCl, 36.5%) was supplied by Riedel-de Haen AG. Formaldehyde (HCHO, extra pure grade) and acetone (ACS grade) were supplied by Union Chemical Works Ltd. For core/sheath melt-spinning technique, the compatibility and spin ability of these polymers are the main selection criteria.

Preparation of core/sheath fiber

Core/sheath fiber was a specific fiber in which the primary core component was fully and evenly covered by the second sheath component. The first stage of melt-spinning was performed with the aid of two single-screw extruders (model GT-25, Plabor, Japan) joined to a core/sheath spinneret containing 48 orifices. The extruders were set with five different temperature zones ranging from 150 to 220 °C along the extruder barrel. The PP resin was extruded into the core part and the PF/PE mixture was extruded into the sheath part of the core/sheath spinneret, as schematically described in Fig. 1. The PF loading was 5–20 wt% in CSF and is designated as CSF-*N*, where the number *N* indicates the weight percent of the PF; the same sample designation applies to CFP-*N* and CNF-*N* as well.

Preparation of carbon fiber precursor

In the second stage, the CFP after melt-spinning was stabilized in a solution containing HCl (12 wt%) and HCHO (18 wt%); it was later neutralized with aqueous ammonia, washed with water, and dried at 80 °C for 1 h to form CFP. The crosslinking reaction between the linear PF chains took place during this stabilization stage. The CFP was finally extracted by acetone for 24 h, washed with water, and then dried at 80 °C for 1 h.

Preparation of carbon nanofiber

Finally in the third stage, the CFP was converted into CNF after removing the PP and PE during the high temperature carbonization process at 800 °C for 1 h in a furnace under nitrogen atmosphere with a heating rate 5 °C/min from ambient temperature to 800 °C.

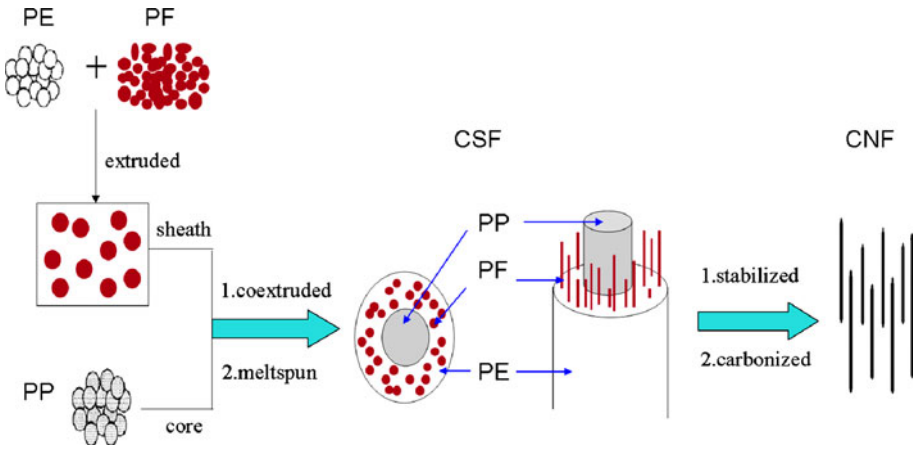

Fig. 1 Schematic showing the process of CNF

Characterization

The mechanical properties of CSF were measured with a single fiber tester (Fafegraph HR and Vibromat ME, Textechno). Values of linear density, tenacity, and elongation were averaged with ten measurements for each sample. Microstructure of CNF was analyzed by scanning electron microscopy (SEM, JSM-5200, JEOL™) operated at 20 kV. Thermal behavior of CSF and CFP was measured by a thermogravimetric analyzer (TGA, Pyris™ 1, Perkin-Elmer) scanning from room temperature to 800 °C with a heating rate of 10 °C/min and under nitrogen atmosphere. The Raman spectrometer used here was a Horiba Jobin-Yvon T64000 instrument for microstructure analysis. Samples for Raman were excited under a 532 nm laser source at 10 mW and under ambient conditions. The scattered light was collected in the back scattering configuration. The analyzed region was directly visualized through a 100× microscope objective. The spectra were recorded at a 0.8 cm^{-1} resolution and averaged over three scans to improve the signal-to-noise ratio.

Crystalline phases were determined by X-ray diffractometry (XRD, D-5000, Siemens) with Cukα radiation (0.154 nm) and fixed slit operating at 40 kV and 30 mA. Samples were ultrasonicated in ethanol and filtered on holey carbon grids before the microstructure observation by analytical scanning transmission electron microscopy (AEM, JEM-3010, JEOL™) and field emission gun high resolution transmission electron microscopy (FEG-HRTEM, Tecnai™ G2 F20, FEI/Philips); the latter was operated at 200 kV.

Results and discussion

Core/sheath fiber

The small PF particles with diameter of few micrometers embedded in the PE sheath of CSF were drawn and elongated to become thinner and finer. Thus, a multitude of ultra-fine fibers oriented in the fiber drawing direction in PE matrix can be expected. Summarized in Table 1 are the mechanical properties of samples CSF-*N*. The linear density, expressed in dtex (the mass in gram per 10,000-m long fibers, the SI unit used in synthetic fiber industries), remains practically the same regardless of the various PF loading in CSF series. This can be rationalized that the density of the individual polymer used in the composites has roughly the same density. Meanwhile, the tenacity (expressed in cN/dtex, the force in centi-Newton required per unit linear density at the break point, also the SI unit used in synthetic fiber industries) decreases and the elongation at break increases with increasing PF loading in the CSF series. This is mainly due to the reinforcement role of the PF which inhibits the molecular orientation in the PE phase and thus increases the amorphous regions in the composite fibers, resulting in a reduced brittleness. SEM image (Fig. 2) of sample CSF-10 after acetone extraction reveals an irregular and rough surface which suggests the existence of the etched PF fibrils; the size of the cavities is less than 1 μm, as marked by the arrow. It also reveals that the PF fibrils are oriented parallel to the surface of CFP. As a contract, a smooth surface without discernible cavities is observed for sample CSF-0 in Fig. 2a. On the other hand, no cavity is present on the surface of sample CFP-20 (Fig. 2c) after acetone extraction. Apparently, the cross-linking reaction taking place between the linear PF chains

Table 1 Mechanical properties of samples CSF-*N*

Sample	Linear density (dtex)	Tenacity (cN/dtex)	Elongation (%)
CSF-0	6.3 ± 1.1	0.88 ± 0.09	224 ± 113
CSF-5	5.8 ± 0.8	0.77 ± 0.19	343 ± 187
CSF-10	5.8 ± 1.1	0.89 ± 0.09	518 ± 53
CSF-15	5.8 ± 1.0	0.67 ± 0.20	500 ± 96
CSF-20	6.2 ± 0.9	0.49 ± 0.12	524 ± 44

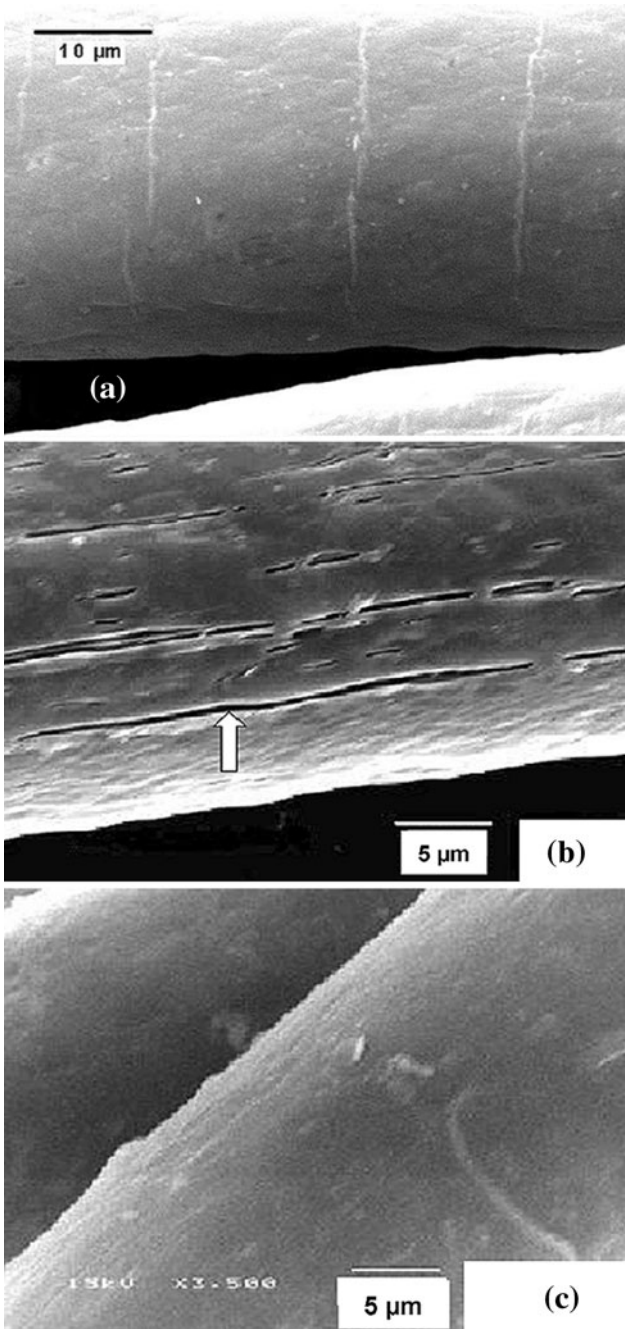

Fig. 2 SEM images on the fiber surface after acetone extraction; **a** CSF-0, **b** CSF-10, and **c** CFP-20

plays an instrumental role of reinforcement in preventing the CSF from solvent attacking.

Carbon fiber precursor

It is reported that the carbocations $^{+}CH_2OH$ originated from the curing solution were able to diffuse into the interior of PF fibrils during the stabilization stage, making possible the crosslinking reaction between phenolic rings

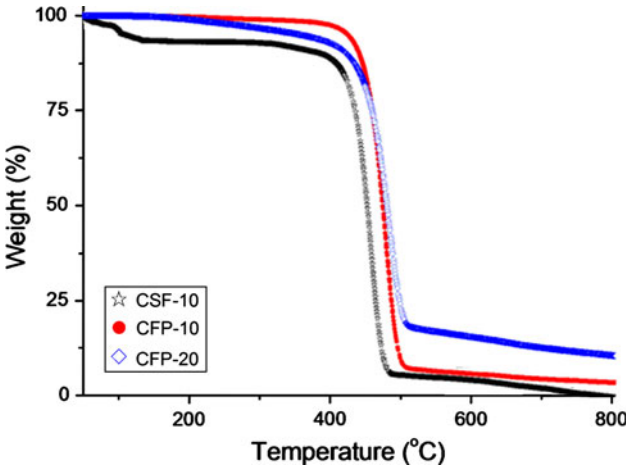

Fig. 3 TGA traces of samples CSF-10, CFP-10, and CFP-20

by methylene bridges [23]. The effect of this stabilization process can be illustrated by TGA traces in Fig. 3. Sample CSF-10 displays a major weight loss at 400 °C and is completely degraded at 800 °C. Meanwhile, the residual weight at 800 °C is 5.5 and 12.5 wt% for samples CFP-10 and CFP-20, equivalent to a CNF yield of 55.0 and 62.5% from the original raw PF content, respectively. It is the crosslinked structure within the PF resin that makes the CFP more thermally resistant, thus ensuring a more stabilized carbonaceous structure during the subsequent carbonization.

Carbon nanofiber

It is clear that only the PF resin is left after the removal of PE and PP, and the PF resin is transformed into CNF during the carbonization stage. When the CNF thus prepared was weighted and compared to the original PF content, a CNF yield of 43.8 and 47.6% for sample CNF-10 and CNF-20 are obtained, respectively, about 10–15% less than those measured by TGA where the samples which were not subjected to isothermal heating at 800 °C. SEM images of sample CNF-10 in Fig. 4a show long and winding fibers having diameter of 100–600 nm and length greater than 80 μm. A more regular CNF diameter of 200–300 nm was reported adopting a solvent process to prepare the core–shell microspheres [17–22]. In addition, the CNFs seem to be regularly oriented into bundles and the bundles curl up to become rolls of wavy long fibers. Note that the surface of the fibers under SEM (Fig. 4b) is clean and smooth, although not as flat as expected.

TEM image of sample CNF-10 in Fig. 5a displays a very smooth and clean surface with fiber diameter 100–600 nm, consistent with the SEM findings. A closer look under higher magnification in Fig. 5b reveals a cup-shaped tip and also a nano-scaled roughness on the surface

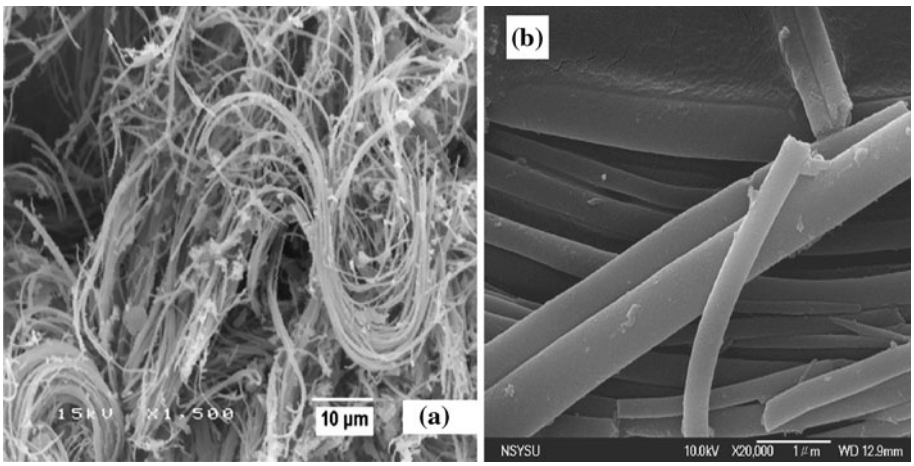

Fig. 4 SEM images of sample CNF-10; **a** low and **b** high magnifications

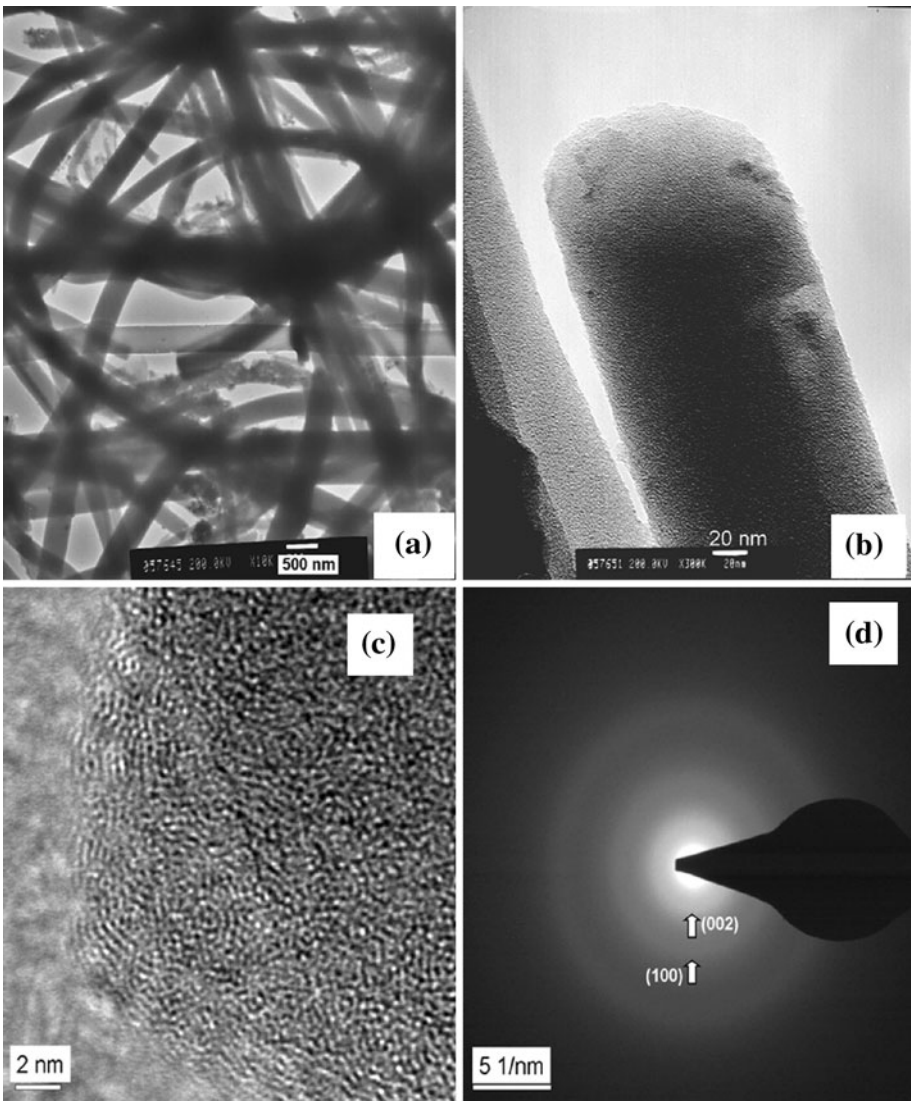

Fig. 5 TEM and HRTEM images of sample CNF-10; **a** low and **b** high magnifications, **c** high resolution on the fiber tip in **b** showing the graphite fringes, and **d** the SAED pattern

with some occasional concavities. Certain graphite fringes can be identified on the CNF fiber surface, as shown in the high resolution image in Fig. 5c, due mainly to the oriented PF fibrils along the fiber direction during the spinning and drawing stage. The selected area electron diffraction (SAED) pattern taken on the fibril tip (Fig. 5d) indicates

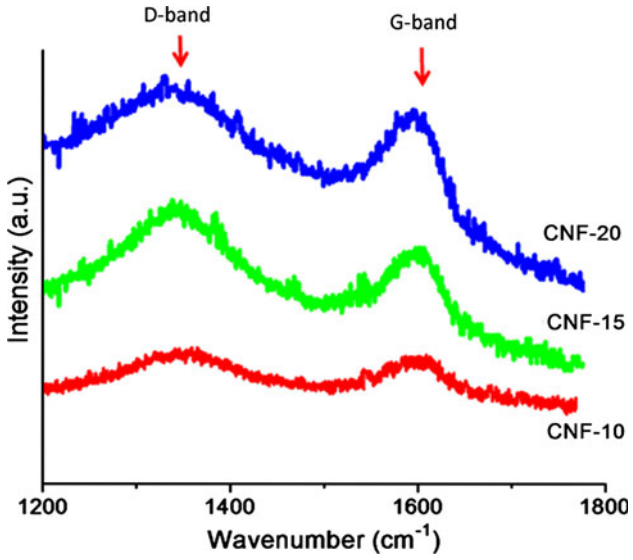

Fig. 6 Raman spectra of samples CNF-*N*

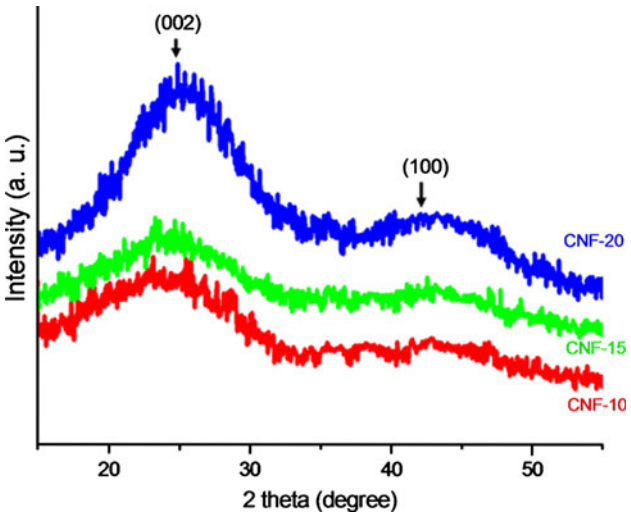

Fig. 7 XRD profiles of samples CNF-*N*

three thin diffraction rings around the center spot, suggesting the presence of the ordered graphitic particles and a disordered random carbon structure. This result matches very well with the findings from Raman spectroscopy (a high I_D/I_G band intensity ratio) and XRD [a broad (002) peak and a weak (100) peak], as stated below. Thus, the CNF prepared in this study can be characterized as a mixed-phase carbon material having graphitic particles embedded homogeneously in an amorphous carbon matrix [24, 25].

Raman peaks of CNF at 1350 and 1600 cm^{-1} are typically associated with the D band and G band of the carbon material, respectively (Fig. 6). The D band near 1350 cm^{-1} is due to the disordered portion and small crystal sizes of the carbons not typically found in those highly oriented pyrolytic graphite (HOPG); whereas the G band near 1600 cm^{-1} is indicative of the less-ordered graphitic crystallites of the carbons, as compared to the G band of HOPG at 1580 cm^{-1} [25–27]. The degree of crystallinity can also be quantified by the intensity ratio $R = I_D/I_G$, where I_D and I_G are the integrated intensity of the D and G band, respectively [25, 26]. This R value is calculated and found to be 1.34 for sample CNF-20 in Fig. 6, implying a rather less crystallinity when compared to that of the crystalline graphite with $R = 0.1$–0.3. This result is consistent not only with the findings from the previous findings by HRTEM and SAED, but also with the XRD described below.

Investigation on the microstructure by XRD (Fig. 7) provides further evidence about the dual phase nature of the CNF studied. A broad (002) peak at $2\theta = 23$–$25°$ is strongly indicative of an amorphous carbon structure; whereas the broad and weak (100) peak near $2\theta = 41$–$43°$ suggests the presence of the ordered graphitic particles. The interlayer distance between the graphene planes (d_{002}) determined from the Bragg's law is 0.355 nm for the ordered graphitic particles of sample CNF-20, which is larger than that of the ideal crystalline graphite ($d_{002} = 0.335$ nm). This indicates that the CNF prepared in this study exhibits a less-ordered carbon structure. Apparently, a higher carbonization temperature than 800 °C is necessary to get a more ordered turbostratic graphite structure [28].

Conclusions

We have demonstrated in this study a novel core/sheath melt-spinning approach to prepare the CNF with diameter 100–600 nm. A CSF with PP as the core and PF–PE as the sheath was coextruded and melt-spun in the first step; it then proceeded with a stabilization process to induce the chemical crosslinking reaction within the PF fibers to form the CFP. Then, the precursors were finally converted to the CNF by carbonization at 800 °C. The linear density of CSF remains practically the same regardless of the various PF loading in CSF series; whereas the tenacity decreases and the elongation at break increases with increasing PF loading in the CSF series. This is mainly due to the reinforcement role of the PF which inhibits the molecular orientation in the PE phase and thus increases the amorphous regions in the composite fibers. From TGA analysis, it is found that the carbocation-induced crosslinking reaction between phenolic rings by methylene bridges within the PF resin makes the CFP more thermally resistant, thus ensuring a more stabilized carbonaceous structure during the subsequent carbonization. Both SEM and TEM images

of CNF reveal long and winding fibers having a diameter 100–600 nm and a length greater than 80 μm. With a yield of ~45% based on its raw material PF, the fibers with clean and smooth surface are regularly oriented into bundles and the bundles curl up to become rolls of wavy long fibers. Results from XRD, Raman spectroscopy, and SAED indicated that the CNF is a mixed-phase carbon material with graphitic particles embedded homogeneously in an amorphous carbon matrix.

Acknowledgements This study was sponsored in part by San Fang Chemical Industry Co, Ltd, Taiwan.

References

1. Inagaki M, Radovic LR (2002) Carbon 40:2279
2. Inagaki M, Kaneko K, Nishizawa T (2004) Carbon 42:1401
3. Ramirez AP (2005) Bell Labs Tech J 10:171
4. Mordkovich VZ (2003) Theor Found Chem Eng 37:429
5. De Jong KP, Geus JW (2000) Catal Rev Sci Eng 42:481
6. Harris PJF (1999) Carbon nanotubes and related structures. Cambridge University Press, United Kingdom, p 1
7. Armentano I, Del Gaudio C, Bianco A, Dottori M, Nanni F, Fortunati E et al (2009) J Mater Sci 44(18):4789. doi: 10.1007/s10853-009-3721-3
8. Blackman JM, Patrick JW, Arenillas A, Shi W, Snape CE (2006) Carbon 44:1376
9. Che G, Lakshmi BB, Fisher ER, Martin CR (1998) Nature 393:346
10. Endo M, Kim YA, Hayashi T, Takeda T, Miyashita T, Dresselhaus MS et al (2001) Carbon 39:2003
11. Keidar M, Waas AM (2004) Nanotechnology 15:1571
12. Scott CD, Arepalli S, Nikolaev P, Smalley RE (2001) Appl Phys A Mater Sci Process 72:573
13. Chronakis IS (2005) J Mat Process Technol 167:283
14. Zhou FL, Gong RH (2008) Polym Int 57:837
15. Chung GS, Jo SM, Kim BC (2005) J Appl Polym Sci 97:165
16. Kim DK, Park SH, Kim BC, Chin BD, Jo SM, Kim DY (2005) Macromol Res 13:521
17. Patel N, Okabe K, Oya A (2002) Carbon 40:315
18. Oya A, Naoto K (2000) Carbon 38:1141
19. Hulicova D, Oya A (2003) Carbon 41:1443
20. Okabe K, Yao T, Shiraishi N, Oya A (2005) J Mater Sci 40:3847. doi:10.1007/s10853-005-2561-z
21. Hulicova D, Hosoi K, Kuroda S, Oya A (2005) Carbon 43:1246
22. Hulicova D, Yamamoto M, Yokoyama T, Oya A (2004) Key Eng Mater 264–268:2275
23. Liu CL, Guo QG, Shi JL, Liu L (2005) Mater Chem Phys 90:315
24. Kishore N, Sachan S, Rai KN, Kumar A (2003) Carbon 41:2961
25. Ermolieff A, Chabli A, Pierre F, Rolland G, Rouchon D, Vannuffel C et al (2001) Surf Interface Anal 31:185
26. Yang KS, Kim C, Park SH, Cho JI, Lee DY, Lee WJ et al (2004) J Raman Spectrosc 35:928
27. Boudou JP, Paredes JI, Cuesta A, Martinez-Alonso A, Tascon JMD (2003) Carbon 41:41
28. Kasahara N, Shiraishi S, Oya A (2002) Carbon 41:1654